AIAA JOURNAL
Vol. 40, No. 12, December 2002

Numerical Investigation of High-Enthalpy Flows Generated by Expansion Tube

Hirotaka Otsu*
Shizuoka University, Hamamatsu 432-8561, Japan
Takashi Abe†
Institute of Space and Astronautical Science, Sagamihara 229-8510, Japan
and
Yasuyuki Ohnishi,‡ Akihiro Sasoh,§ and Kazuyoshi Takayama¶
Tohoku University, Sendai 980-8577, Japan

We have investigated by numerical simulation the hypersonic and high-enthalpy flows around a reentry body, which Sasoh et al. examined experimentally in an expansion tube facility (Sasoh, A., Ohnishi, Y., Ramjaun, D., Takayama, K., Otsu, H., and Abe, T., "Effective Test Time Evaluation in High-Enthalpy Expansion Tube," *AIAA Journal*, Vol. 39, No. 11, 2001, pp. 2141–2147). For the experiment, the evaluation of the timing at which the test flow is attained and the freestream condition of the test flow are the most crucial issues. Therefore, it was necessary to validate these issues in another way, rather than the simple estimation by Sasoh et al. based on the pressure and spectral emission measurements. Thus, the experimental result was intensively investigated compared to the numerical result based on the experimentally determined freestream condition. In the context of the thickness of the radiating shock layer for which the experimental result was obtained, the results show a good agreement, and we can conclude that the test time and the freestream condition in the experiment are reasonably estimated.

Nomenclature

$k_{b,r}$ = backward reaction rate coefficient for chemical reaction r
$k_{f,r}$ = forward reaction rate coefficient for chemical reaction r
M_s = molecular weight of chemical species s
N_S = the number of chemical species in the system
X_s = molar concentration of chemical species s
$\alpha_{s,r}$ = stoichimetric coefficient for products in chemical reaction r
β = relaxation parameter for diagonal implicit method
$\beta_{s,r}$ = stoichimetric coefficient for reactants in chemical reaction r
ρ_s = density of species s
ω_s = mass rate of production of species s

Subscripts

s = species s
r = chemical reaction r

I. Introduction

THE program MUSES-C for a sample return mission from an asteroid is in progress at the Institute of Space and Astronautical Science (ISAS).[1] The spacecraft is scheduled to be launched in 2002, and the capsule with a sample of the asteroid soil to return to the Earth in 2006. In the MUSES-C program, the capsule is designed to enter directly from the interplanetary orbit into the Earth atmosphere at a superorbital speed to reduce the mass and the complexity of the vehicle system. In return for these reductions, we must solve some difficulties, the most important one of which is that the capsule must be exposed to a very severe aerodynamic heating condition. Because the capsule must be protected from such severe aerodynamic heating, the development of the thermal protection system (TPS) is one of the key technologies for the superorbital reentry flight.

For an accurate design of the TPS, the aerodynamic heating rate must be predicted accurately. Therefore, ground-testing methods should be established, in parallel to the numerical prediction method. Currently, several kinds of ground-test facilities are available. Among these, one of the most conventional facilities is the shock tunnel, which Hornung[2] used to perform an experiment for a hypersonic flow and reported the interferometric measurement of the density distribution around a cylindrical model. In response to the experiment, Park and Yoon[3] performed numerical simulations and reported good agreement between the experiment and simulations. However, the flow speed attained in the shock tunnel is still a suborbital reentry speed, and, in addition, the freestream flow still has a nonequilibrium nature caused by a rapid expansion through a nozzle. Therefore, such a conventional facility is not ideal for the testing in the superorbital reentry flow condition.

Other than the shock tunnel, several ground-testing methods are already available for hypersonic flow simulation. However, in most cases, the required velocity and enthalpy for the superorbital reentry condition are not achievable. An expansion tube is one of the methods that has potential to become an ideal testing method for hypersonic flow simulation. In Ref. 4 it is reported that this method could create the flow condition close to the superorbital reentry and, thus, showed its potential to be an ideal testing method for the superorbital reentry flow simulation. A disadvantage of this method is its inherent impulsive nature, which, however, could be covered by the current development of the high-speed diagnostic technique. Another disadvantage is related to the complexity of identifying the freestream flow. That is, the freestream flow is barely attained, for only a short period, after a rather complex unsteady flow generated from the initial setup. Also, the freestream condition is determined by taking into account the complex interactions between several expansion and compression waves generated during an operation. Hence, it is quite important to identify the timing of test time in which the freestream flow is attained and to determine the

Received 20 May 2001; revision received 22 April 2002; accepted for publication 8 July 2002.

*Research Associate, Department of Mechanical Engineering, 3-5-1 Johoku. Member AIAA.
†Professor, Gas Dynamics Branch, Division of Space Transportation, 3-1-1 Yoshinodai. Associate Fellow AIAA.
‡Graduate Student, Shock Wave Research Center, Institute of Fluid Science, 2-1-1 Katahira, Aoba-ku.
§Associate Professor, Shock Wave Research Center, Institute of Fluid Science, 2-1-1 Katahira, Aoba-ku. Associate Fellow AIAA.
¶Director and Professor, Shock Wave Research Center, Institute of Fluid Science, 2-1-1 Katahira, Aoba-ku. Senior Member AIAA.

conditions for the freestream flow. Once the test time and the flow conditions are reliably identified, an expansion tube could become a reliable testing method for hypersonic flows. Recently, Sasoh et al.[5] conducted an experiment on the expansion tube to evaluate the test time and reported a method to establish it in the expansion tube. In the experiment, they obtained instantaneous pictures of a radiating shock layer formed around the body inserted in the hypersonic flow. Even though the flow speed in the experiment is barely above a suborbital reentry speed, it was concluded that their facility shows good potential to be extended to superorbital reentry testing. Their method to evaluate the test timing, however, is based on a simple estimation using the pressure and spectral emission measurements, and, therefore, it is necessary to validate it somehow.

For this purpose, a numerical simulation technique is suitable because it is an alternative method for simulating superorbital reentry flow. After sufficient validations, together with the experimental results, the numerical simulation could become a strong tool to predict the hypersonic reentry flow. Related to the MUSES-C program, a numerical simulation code has been developed[6,7] for superorbital reentry flow and has been applied to the flowfield prediction around the MUSES-C reentry capsule. In the code, the chemical reaction model for the numerical simulation is based on the Park model,[8] which was constructed for application to the intermediate reentry speed, slightly higher than a suborbital reentry but lower than a superorbital reentry. It is believed that the Park model[8] can sufficiently predict the flow behavior at the intermediate reentry velocity. The validation of the present simulation code was carried out by using existing results, including Hornung's experimental result,[2] and the result was promising. Therefore, in this study, we attempt to examine the experimental data obtained by Sasoh et al.[5] using the developed simulation code. Thus, we thoroughly compare the numerical flow based on the uniform flow data determined experimentally with the visualization data obtained experimentally. This may validate the method for the expansion tube to establish the timing of the freestream and the conditions for it.

II. Aerothermal Models: Governing Equations

The governing equation of the thermally and chemically nonequilibrium flow can be represented by[9]

$$\frac{\partial \boldsymbol{U}}{\partial t} + \frac{\partial \boldsymbol{F}_j}{\partial x_j} = \boldsymbol{S} \tag{1}$$

where $\boldsymbol{U}$, $\boldsymbol{F}_j$, and $\boldsymbol{S}$ are the vector of conserved quantities, the flux vector, and the source vector, respectively. Park's two-temperature model[10] for thermal nonequilibrium is considered. In this model, translational and rotational temperatures are represented by a common temperature T, whereas a vibrational temperature of each molecule, an electronic excitation temperature of each species, and a translational temperature of free electrons are represented by a common temperature T_V. The vector of conserved quantities $\boldsymbol{U}$ is

$$\boldsymbol{U} = (\rho_s, \rho u_j, \rho e, \rho e_V)^t \tag{2}$$

where ρ_s is the density of each species, u_j is a flow velocity component, e is the total energy of per unit mass, and e_V is the summation of vibrational energy of each molecule, translational energy of free electron, and electronic excitation energy per unit mass. The vibrational energy of each species is calculated using the harmonic oscillator model, whereas the first two terms of the partition function are considered for the electronic excitation energy of each species.

The relaxation time of each species for a translational–vibrational energy relaxation is calculated using the semi-empirical correlation proposed by Millikan and White[11] and the correction term suggested by Park[8] is considered. As for the molecular process in which a certain amount of energy is removed at dissociation or is added at the recombination of molecules, the amount of the energy is set to be 30% of the dissociation energy of each molecules,[12] according to the standard "preferential dissociation model."[13]

The finite rate chemical reaction model is one of the most important parts of a numerical simulation of a hypersonic and high-enthalpy flow. This is because the dissociation and ionization process of chemical species, requiring a large amount of energy, leads not only to a rapid decrease of temperatures in the shock layer but also to a significant change of the shock shape and location. For dissociating air, we considered 11 species consisting of N, O, N_2, O_2, NO, N^+, O^+, N_2^+, O_2^+, NO^+, and e^-. For rate coefficients for the chemical reaction between them, Park's reaction model[8] for air species is considered.

The viscosity of each species is evaluated by a curve-fitting method based on the tabulated data.[14] The heat conductivity of the translational, vibrational, and electron temperature are calculated using an Eucken's relation (see Refs. 15 and 16). The total viscosity and conductivity are calculated using Wilke's semi-empirical mixing rule.[17] The diffusion coefficients between the species are evaluated based on the viscosity, assuming the Schmidt number of 0.5. The diffusion coefficients for ions are doubled to take into account the ambipolar diffusion effect, and a local charge neutrality is assumed to be kept throughout the flowfield.

III. Numerical Methods

A. Numerical Scheme

In the simulation, the strong shock wave and, therefore, a shock layer with a complex chemical nonequilibrium are expected to appear in front of the reentry body. Generally speaking, from the standpoint of stability of the numerical simulation, the stronger the shock wave is, the tougher the simulation is. Therefore, the numerical scheme to simulate such a flow must have the following properties: 1) robustness to significant discontinuities such as a shock wave in front of the reentry body and 2) flexibility to the large system of equations such as an 11-species air model.

Considering these requirements, we selected the advection upstream splitting method scheme,[18,19] which is known to be able to capture a stationary discontinuity such as a shock wave with less numerical dissipation and which is strong enough to calculate the strong shock waves and expansions. Additionally, its flux splitting scheme is preferred for application to a large system of equations like the present one.

B. Diagonal Implicit Method

The stiffness problem, inherent to strong dissociation and ionization reactions, requires us to incorporate a kind of numerical relaxation method. One of the relaxation methods is the point implicit method,[20] which treats the convective terms explicitly and solves only the source terms implicitly. This method is expressed as

$$\left[I - \Delta t \frac{\partial \boldsymbol{S}_j}{\partial \boldsymbol{U}_s}\right] \Delta \boldsymbol{U} = -\Delta t R^n, \qquad \Delta \boldsymbol{U} = \boldsymbol{U}^{n+1} - \boldsymbol{U}^n \tag{3}$$

where R^n is the residual calculated explicitly at time step n. Certainly, this method can remove the stiffness problem, but still needs an inversion of the matrix $[I - \Delta t \partial \boldsymbol{S}_j / \partial \boldsymbol{U}_s]$, which consumes computational time. If this matrix is approximated to the diagonal matrix, computational cost can be reduced. For this purpose, Eberhardt and Imlay[21] proposed the following approximation:

$$\left[I - \Delta t \frac{\partial \boldsymbol{S}_j}{\partial \boldsymbol{U}_s}\right] \approx \left[I + \mathrm{diag}\left(\frac{\Delta t}{\tau_s}\right)\right] \tag{4}$$

$$\frac{1}{\tau_s} = \beta_c \left[\sum_j \left(\frac{\partial w_s}{\partial \rho_j}\right)^2\right]^{\frac{1}{2}} \tag{5}$$

where β_c is the relaxation parameter. This method can reduce the inversion process. Nevertheless, this method still needs to evaluate lots of partial derivatives of chemical source terms, which is still a time-consuming process. We should remember that, in our case, for example, 11^2 partial derivatives for an 11-species air model must be calculated. To solve this problem, in our code, the following simplified method is employed. Let us consider the chemical reaction source term that is expressed as

$$w_s = M_s \sum_r (\beta_{s,r} - \alpha_{s,r}) \left[k_{f,r} \prod_j X_j^{\alpha_{j,r}} - k_{b,r} \prod_j X_j^{\beta_{j,r}}\right]$$

where $\alpha_{s,r}$ and $\beta_{s,r}$ are constants and less than 3. For the present numerical simulation code, the partial derivative of this term is approximated in the following manner:

$$\frac{\partial w_s}{\partial \rho_j} = \sum_r (\beta_{s,r} - \alpha_{s,r}) \left[\frac{\alpha_{j,r}}{X_j} k_{f,r} \prod_j X_j^{\alpha_{j,r}} - \frac{\beta_{j,r}}{X_j} k_{b,r} \prod_j X_j^{\beta_{j,r}} \right] \approx \frac{w_s}{\rho_s}$$

Therefore, we approximate the relaxation term $1/\tau_s$ by

$$1/\tau_s \approx \beta \times N_S \times |w_s/\rho_s| \tag{6}$$

Using the last expression, we can greatly reduce the computational time to calculate the partial derivatives of the chemical source term. According to our experience, the value β must be larger than 0.3 to avoid a numerical instability. Because the larger value of β means a slow convergence, the recommended value for β is between 1.5 and 0.3. In the calculation, the β value of 1.5 was used initially, and it can be reduced to 0.3 gradually as the calculation proceeds. Note that the value of β is considered to be problem dependent. However, with the proposed value of β, our code could successfully simulate the flow at a superorbital reentry speed such as MUSES-C reentry conditions. Because the function of β is to overcome the stiffness of the chemical reactions that become more stiff with increasing reentry velocity, and the flow condition at a superorbital reentry is the most severe among most of the reentry flow conditions, the proposed value of β is believed to be applicable to most of the reentry flow simulations.

C. Computational Grid

A computational grid is important to capture clearly the shock front. Because flow properties change drastically at the vicinity of the shock wave, the computational grid points should be distributed densely at the vicinity of the shock front. However, the position and the shape of the shock front cannot be obtained in advance. Thus, in the present calculation, the computational grid points are rearranged every 5000 calculation steps, so that the grid points are distributed densely around the shock wave. That is, the computational grid is optimized automatically as the calculation proceeds. Figure 1 shows the pressure contours and the final computational grid obtained for the flow condition designated as case A in Table 1. Pressure contours are plotted every 40 KPa. As is clearly shown in Fig. 1, computational grid points are distributed densely near the shock wave. To investigate the effect of grid points on the shock shape and shock standoff distance, we prepared two kinds of computational grids, coarse and fine. The coarse computational grid has 30 points along the body surface and 50 points along the line normal to the body surface. The fine computational grid has 30 points along the body surface and 100 points, twice the coarse grid, along the line normal to the body surface. As far as we tested, the difference of shock shape and location between coarse and fine computational grid was negligible. This indicates that the coarse computational grid is sufficient for comparison of the shock shape and location. Thus, in this study, we used the coarse computational grid to reduce the computational cost. For numerical accuracy, we regarded the numerical result as converged after a four order drop of the residual with a final converged computational grid.

Table 1 Freestream condition of expansion tube

Freestream condition	Case A	Case B
Flow velocity, km/s[a]	7.5 ± 0.1	8.5 ± 0.1
Temperature, K[a]	2300 ± 400	1050 ± 200
Static pressure, KPa	9.7 ± 1.2	2.9 ± 0.5
Flow Mach number[a]	8.4 ± 0.6	13.5 ± 1.2
Stagnation enthalpy, MJ/kg[a]	31 ± 0.9	37 ± 0.2

[a]Calculated assuming thermal and chemical equilibrium.

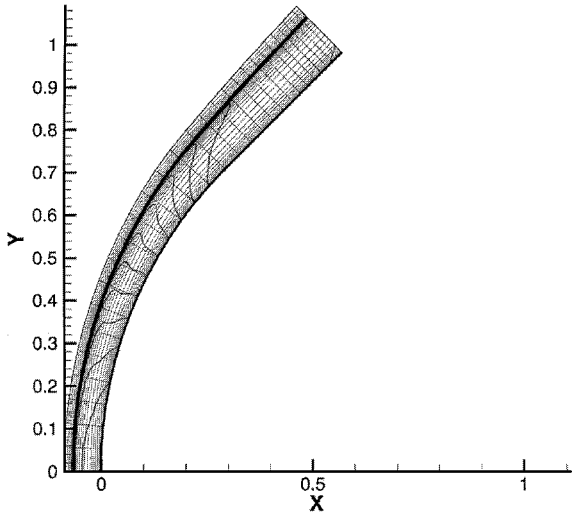

Fig. 1 Converged computational grid for MUSES-C reentry capsule in case A.

D. Boundary Conditions

In this study, the flow is assumed to be axisymmetric. In the calculation, when it is assumed that the flow behind the vehicle can be omitted, only the flow generated in front of the vehicle is calculated. This flow can be realized by imposing a standard outflow boundary condition on the calculation boundary defined at the junction between the front and rear part of the body. A standard inflow boundary condition is imposed on the boundary in front of the body. As a boundary condition on the body surface, the wall temperature is fixed at 2000 K, and the noncatalytic wall condition is imposed. In the experiment, the wall temperature is difficult to measure, and, therefore, we investigated several kinds of boundary condition for wall temperature. As far as we tested in this study, however, the effect of the wall temperature on the thickness of the shock layer was very small.

As for the catalysis of the vehicle surface, we investigated the catalytic effect by applying two limiting conditions, that is, noncatalytic wall and full-catalytic wall. In the noncatalytic wall condition, the mass fraction of each species at the wall is set to be same as the value at the next grid point. In the full-catalytic wall condition, the mass fraction of each species at the wall is set to be the value of the freestream condition. The results showed that the shock standoff distance of the full-catalytic wall condition was 1% smaller than that of noncatalytic wall condition. As shown later, this difference is much smaller than that arising from other uncertainties such as the free stream condition. Thus, in this study, we concluded that the influence from the boundary condition related to the wall catalysis was negligible compared to the uncertainty of the freestream condition. Therefore, only the uncertainty of the freestream condition is employed hereafter.

IV. Results and Discussion

A. Comparison with Experimental Results

The free streamflow conditions, under which the expansion tube[5] experiment was carried out, are given in Table 1 and were obtained, based on the flow measurements, by solving the one-dimensional, thermal and chemical equilibrium flow simulation code together with an initial condition of the tube.[5] This is because, in the expansion tube, the freestream flow is generated as a result of the complex unsteady wave generation starting from the initial setup. The stagnation enthalpies of cases A and B are up to 31 and 37 MJ/kg, respectively. The 1/16-scaled model of the MUSES-C reentry capsule was employed as the reentry body in the experiment, and a full-scale schematic is shown in Fig. 2.

We present the numerical results obtained under the nominal condition of case A. In the experiment, the picture of the shock layer was taken because, at this high-speed freestream flow, the shock layer can radiate because of its high temperature behind the shock wave. Because the radiating shock layer is expected to start to radiate from just behind the shock front, we first compare it with the pressure contour plot numerically obtained. Figures 3 and 4 show photographs of radiating shock layer and contour plot of pressure distribution around the MUSES-C reentry capsule for case A and case B conditions, respectively. The contour lines are plotted at every 40 KPa

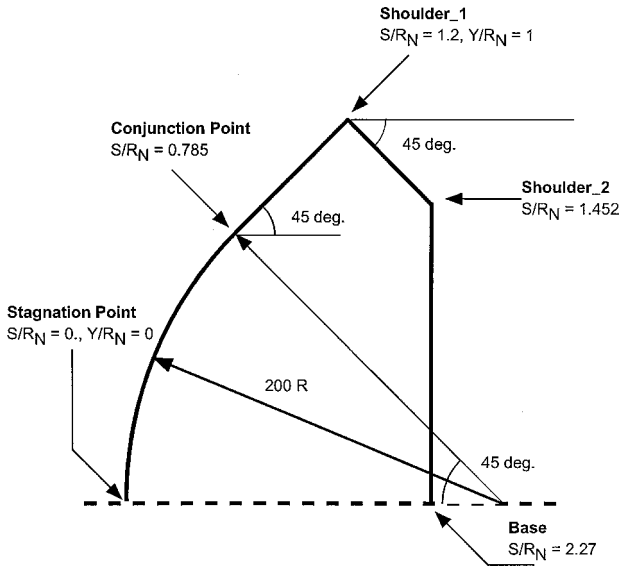

Fig. 2 Schematic geometry of MUSES-C reentry capsule.

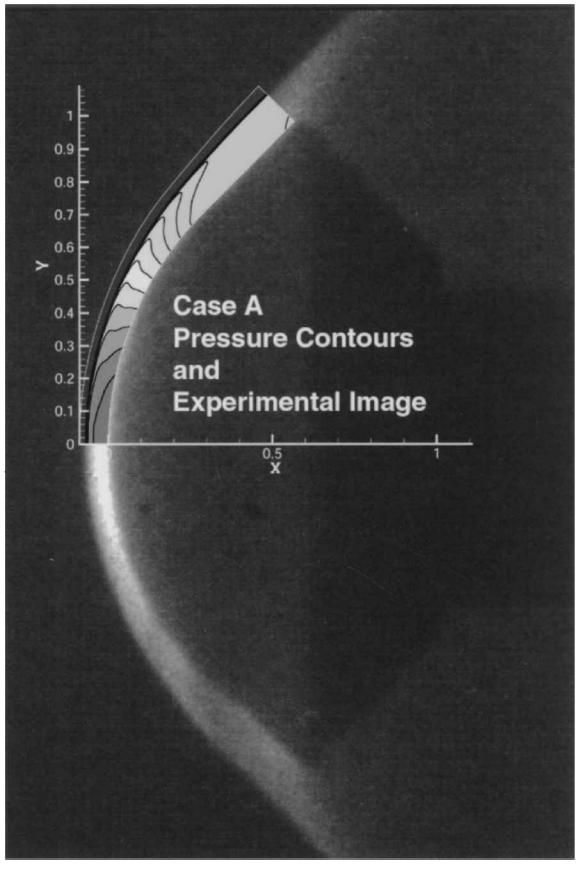

Fig. 3 Comparison of numerical result with experimental image in case A.

in case A and 33 KPa in case B. As shown in case A, the radiating shock layer starts radiating just behind the shock front, which is represented by the sharp pressure rise from the freestream value, and ends at the body surface. This is the case at the vicinity of the stagnation region and also at the other leeward region. In this context, the agreement with experimental results is reasonable. This holds true for both case A and also for case B, where the flow speed is higher in case A.

To compare the result more concisely, we calculated the radiation intensity based on the numerical result. For this purpose, the radiation estimation database SPRADIAN[22] was employed. SPRADIAN is a software package that calculates the emission and absorption

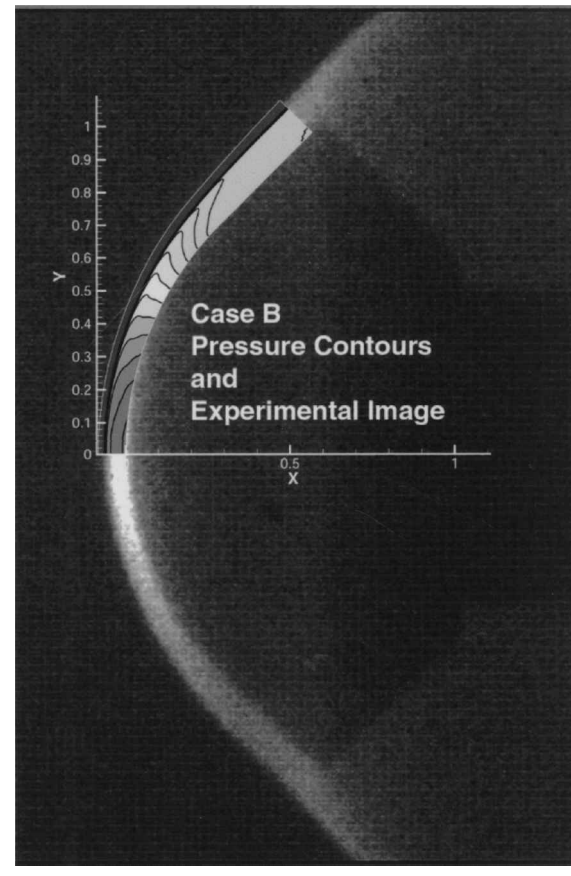

Fig. 4 Comparison of numerical result with experimental image in case B.

coefficient by using flow data such as temperatures and number density of the chemical species. SPRADIAN can cover the range of wavelengths from 500 to 15,000 Å and handle air species and carbon products related to ablation material. The calculation of the radiation intensity by means of SPRADIAN is conducted as follows. First, at every grid point, the emission and absorption coefficients are calculated by using the flowfield data calculated. Then, by use of these coefficients, the radiation intensity is obtained by integrating along the line of sight. Figure 5 shows a comparison between the experimental image of the radiating shock layer and numerical results. The numerical results show the radiation intensity calculated by SPRADIAN. The radiation intensity shown in Fig. 5 is normalized by the maximum value in the shock layer. In Fig. 5, the numerical results show the same tendency as the experimental image. That is, the radiation intensity around the stagnation region is stronger than that in the leeward region, as expected. Near the stagnation region, the thickness and shape of the radiating shock layer agrees very well. On the other hand, in the leeward region, the numerical radiating layer becomes slightly thinner than the experimental one.

B. Flow Characteristics in the Shock Layer

Now let us examine the calculated result and conduct a detailed comparison between the calculated and experimental results, focusing on stagnation region, based on the radiation distribution along the stagnation line. The temperature distribution and the radiation intensity along the stagnation line for cases A and B are shown in Figs. 6 and 7, respectively. The translational–rotational temperature T has one sharp peak due to shock heating. The vibrational–electronic temperature T_V, however, begins to rise due to the temperature relaxation with the translational temperature and has a local maximum point just behind the peak of translational–rotational temperature. The slight drop of the vibrational–electronic temperature just after the peak is due to the energy loss caused by the rapid dissociation of the molecules. After the first peak, there appears a second peak at the vicinity of the body surface. This is due to the drop of the temperature caused by cooling due to the cold-body surface.

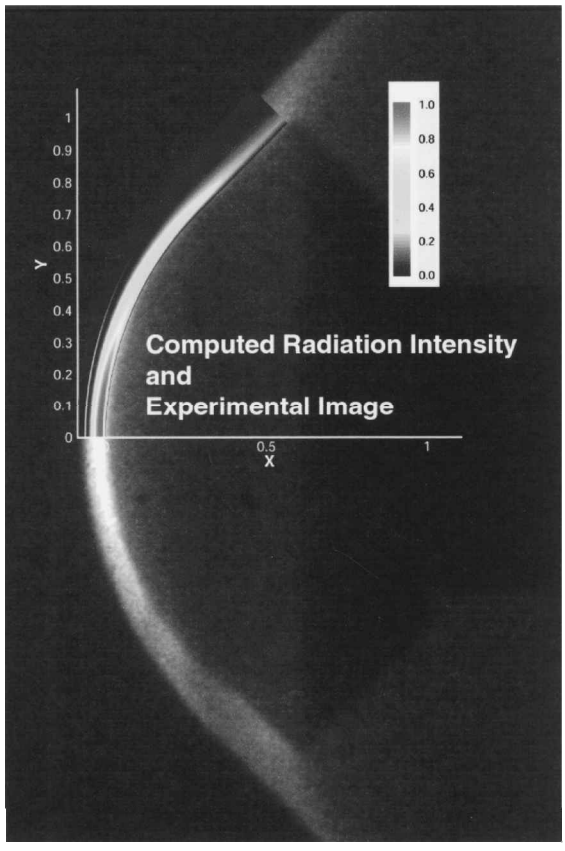

Fig. 5 Comparison of radiation intensity around the MUSES-C reentry capsule in case A.

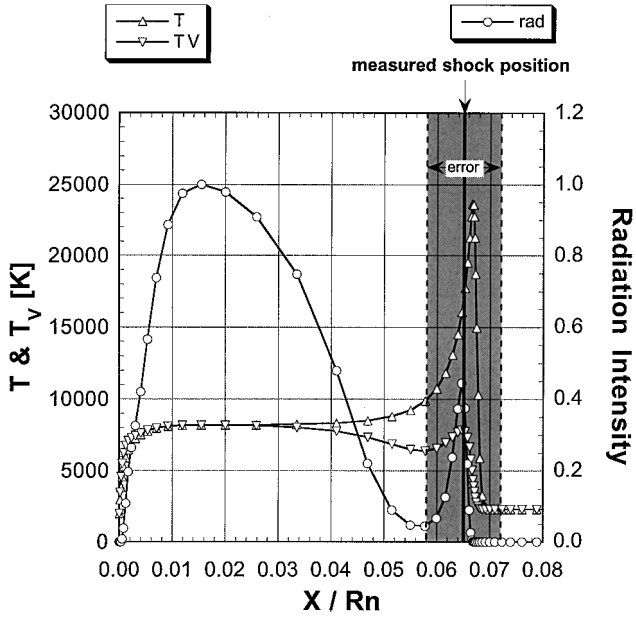

Fig. 6 Distribution of temperatures and radiation intensity along the stagnation line in case A.

The radiation intensity profile shows a good correlation with the vibrational–electronic temperature profile. This is reasonable because, in the present simulation model, the electron temperature, which is responsible to the radiation, is assumed to be equilibrated with the vibrational temperature. The outer edge of the radiating shock layer observed experimentally almost coincides with the first peak of the radiation intensity, which shows a rapid increase from the nonradiating freestream value. In this sense, the outer edge of the radiating shock layer experimentally observed shows good agreement with the one numerically obtained. This agreement is for both cases A and B.

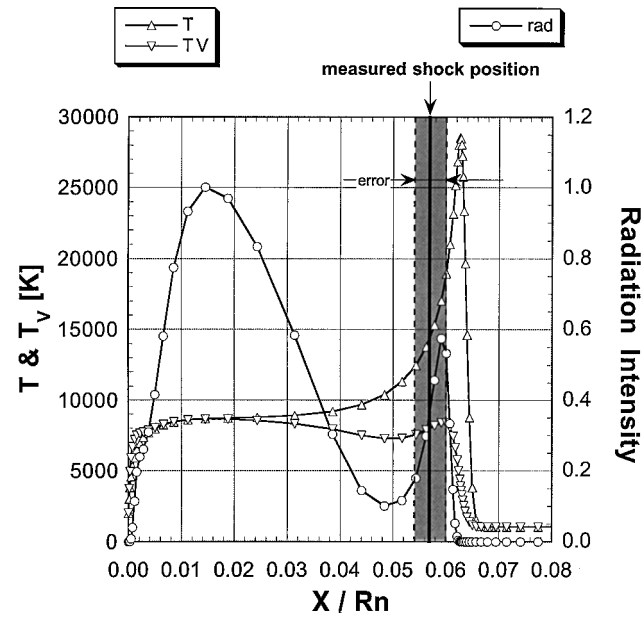

Fig. 7 Distribution of temperatures and radiation intensity along the stagnation line in case B.

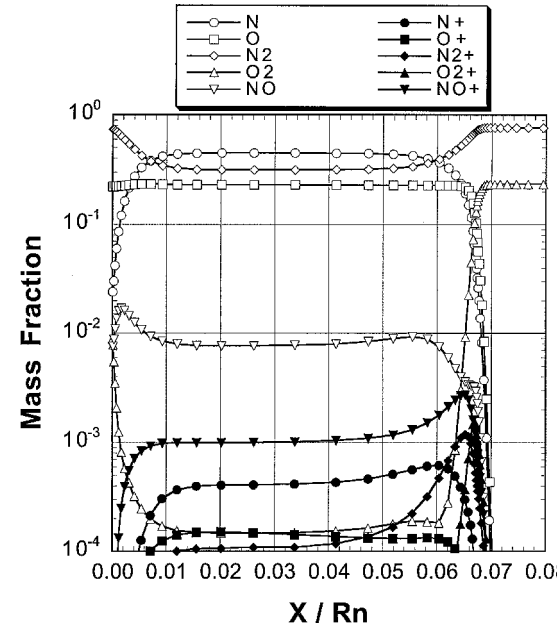

Fig. 8 Distribution of chemical species along the stagnation line in case A.

Apparently, from both the experiment and the numerical simulation, the outer edge of the radiating shock layer depends on the freestream velocity. The faster the freestream velocity is, the thinner the radiating shock layer is. This is caused primarily by the extent of chemical reactions in the shock layer, which become significant along with the higher temperature, that is, the increasing freestream velocity. As shown in Fig. 8, the significant chemical reaction proceeds in the shock layer. The more the freestream velocity increases, the more the chemical reaction proceeds and, as a result, the more dissociation products such as nitrogen atoms are produced as shown in Fig. 9. Because of this, a so-called shock standoff distance decreases, as shown in Figs. 10 and 11, where the temperature distribution profiles are shown. That is, in the context of the temperature profile, the more the free stream velocity increases, the thinner the shock layer thickness is. Because the radiation profile has a good correlation with the vibrational–electronic temperature profile, the radiating shock layer also becomes thinner for the higher freestream velocity. The radiation intensity distribution is shown in Fig. 12.

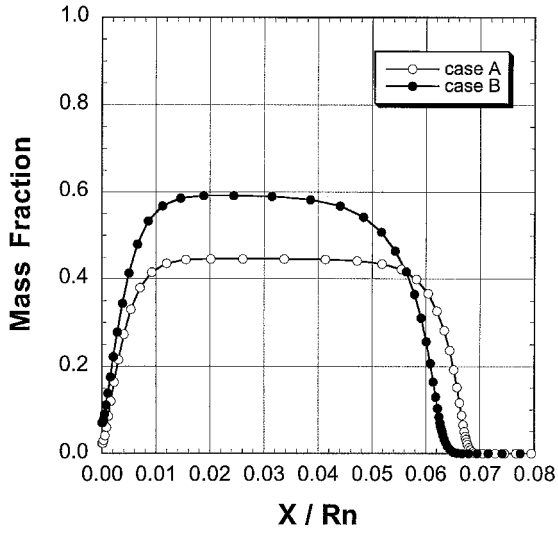

Fig. 9 Distribution of atomic nitrogen along the stagnation line in cases A and B.

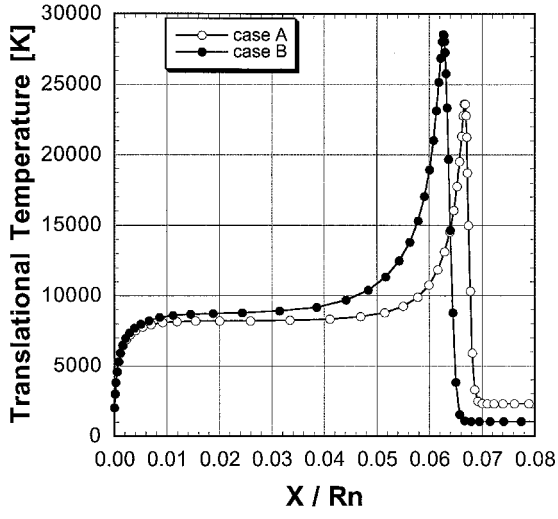

Fig. 10 Translational temperature distribution along the stagnation line in cases A and B.

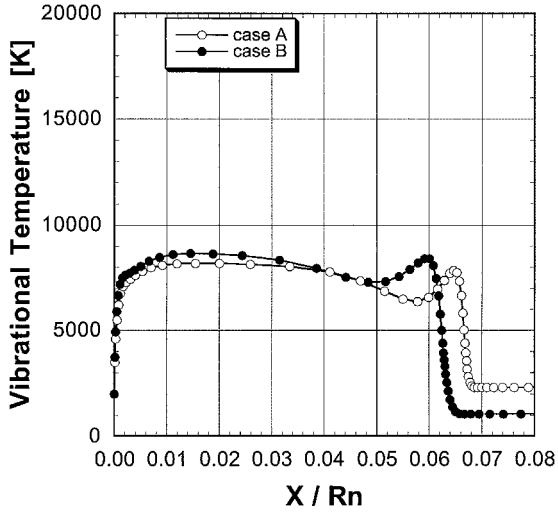

Fig. 11 Vibrational temperature distribution along the stagnation line in cases A and B.

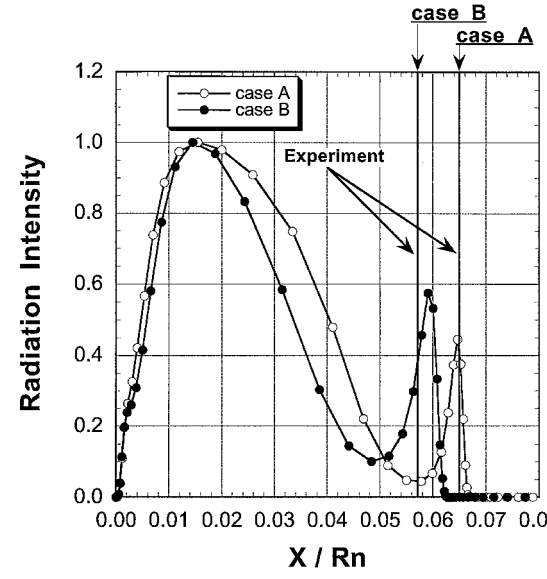

Fig. 12 Radiation intensity distribution along the stagnation line in cases A and B.

C. Sensitivity Analysis

As already mentioned, the freestream flow conditions for the experiment are obtained from the simple calculation based on the measured data. Based on the calculation, the timing of the freestream was evaluated, and the photograph of that radiating shock layer was taken. Because of this situation, the uncertainty in the freestream conditions can not be avoided, as summarized in Table 1. Thus, if the experimental result agrees with the numerical result within the uncertainty, we can conclude the evaluation method of the test timing in the experiment is reasonable.

Before going further, let us define the thickness of the radiating shock layer. Generally speaking, it is difficult to avoid an uncertainty in defining the outer edge of the radiating shock layer. Fortunately, in our case, the radiation intensity shows a sharp rise from a freestream value and has a first peak after the sharp rise. Therefore, we can define the location of the first peak as an outer edge. As shown earlier, the location of the first peak of the radiation almost coincides with the first peak of the vibrational–electronic temperature. Hence, in this section, we define the outer edge of the radiating shock layer as the location of the first peak of the vibrational–electronic temperature, for the numerical simulation result, and compare it to the experimentally observed one. For the comparison, we employ the thickness of the radiating shock layer measured from the body surface to the outer edge of the radiating shock layer.

First, we investigated the effect of the freestream velocity on the thickness for case A. As off-nominal freestream velocities 8000 and 7000 m/s are chosen, while other conditions are kept to be the same as the nominal condition. Figure 13 shows the effect of the freestream velocity on the thickness of the shock layer, which varies almost linearly against the freestream velocity.

Next, we investigated the effect of the freestream temperature on the thickness. Taking the uncertainty into account, the freestream temperature is set to be 1900 and 2700 K, and the freestream velocity is kept to be the nominal value of 7500 m/s. The change of the freestream translational temperature corresponds to the change of the density because the static pressure is considered to be easily measured in the experiment and, thus, to be reliable. If the static pressure is fixed at 9.7 KPa, the freestream density becomes 1.77×10^{-2} and 1.24×10^{-2} kg/m^3, respectively. The nominal freestream density is 1.46×10^{-2} kg/m^3. Figure 14 shows the effect of the freestream temperature on the thickness of the shock layer. The lower freestream temperature produces the thinner shock layer. The thickness varies almost linearly against both the freestream velocity and temperature.

Figure 15 shows the effect of the freestream condition on the thickness of the shock layer. When the uncertainties in the freestream velocity and freestream temperature are taken into account, the present numerical simulation gives the maximum value of the

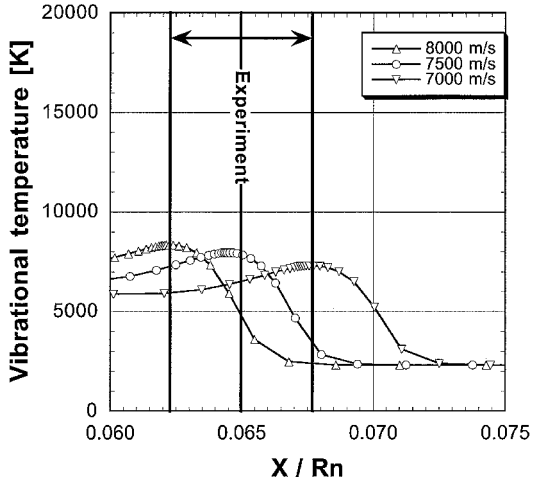

Fig. 13 Effect of freestream velocity on the shock standoff distance.

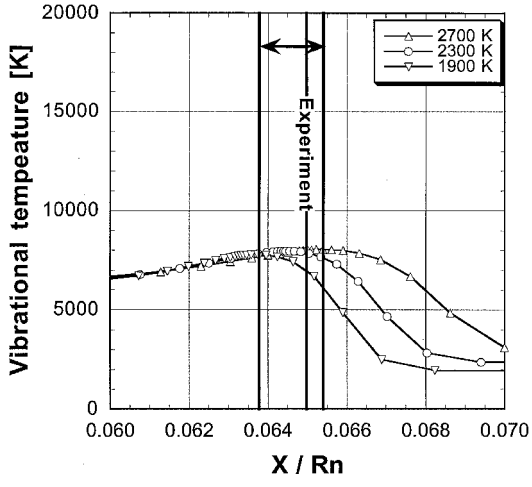

Fig. 14 Effect of freestream temperature on the shock standoff distance.

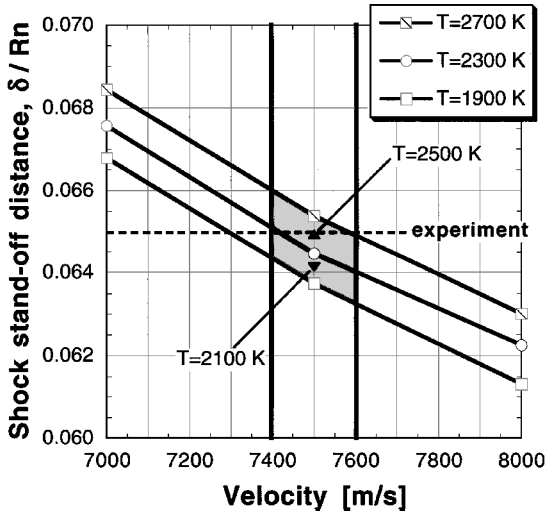

Fig. 15 Effect of freestream condition on the shock standoff distance.

thickness of the shock layer normalized by the nose radius as 0.066 and the minimum value as 0.063.

Hence, according to the calculation, the thickness is between 0.063 and 0.066 considering the uncertainty in the freestream condition. In the experiment, the measured value of the thickness is 0.065 ± 0.007. The uncertainty of the measured value is expected to arise from the difficulty in detecting the outer edge of the shock front due to the resolution of the experimental image. The uncertainty in the measured value, 0.014, is much larger than that of the present numerical simulation, 0.003. Additionally both the maximum and minimum value of the calculated thickness of the shock layer are within the uncertainty of the measured value. In case B, the present numerical simulation predicts the thickness between 0.060 and 0.058, whereas the measured value of the thickness in the experiment is 0.057 ± 0.003.

Therefore, we can conclude that the numerical simulation reasonably validates the experiments conducted by Sasoh et al.[5]

V. Conclusions

By use of a numerical simulation, we have investigated the hypersonic and high-enthalpy flows around a reentry body, which Sasoh et al.[5] examined experimentally by use of their expansion tube facility. For the experiment, an evaluation of the timing at which the test flow is attained and the freestream condition of the test flow are most crucial issues, and, therefore, it was necessary to be validated in another way rather than the simple estimation by Sasoh et al. based on the pressure and spectral emission measurements. For this purpose, the experimental result was intensively investigated and compared to the numerical result based on the freestream condition experimentally determined. In the context of the thickness of the radiating shock layer for which the experimental result was obtained, both the results show a good agreement, and we can conclude that the evaluation of the test time and the freestream condition in the experiment is reasonable.

The result of the present study makes a significant contribution to establish credibility of the expansion tube facility as a reliable testing facility for hypersonic flows. To establish the credibility more firmly, however, further investigations are necessary, such as comparison of surface heat transfer and radiation intensity between the experimental and numerical results and estimation of influence of a thermochemical model on such comparisons. Note that the expansion tube technique has the potential to become a very popular experimental method for hypersonic testing, and the present approach to establish the credibility of the technique for determining the test conditions is crucial for its success.

References

[1]Kawaguchi, J., Fujiwara, A., and Sawai, S., "Sample and Return Mission from Asteroid Nereus via Solar Electric Propulsion," *Acta Astronautica*, Vol. 38, No. 2, 1996, pp. 87–101.

[2]Hornung, H. G., "Non-Equilibrium Dissociating Nitrogen Flow over Spheres and Cylinders," *Journal of Fluid Mechanics*, Vol. 53, Pt. 1, May 1972, pp. 149–176.

[3]Park, C., and Yoon, S., "Fully Coupled Implicit Method for Thermochemical Nonequilibrium Air at Suborbital Flight Speeds," *Journal of Spacecraft and Rockets*, Vol. 28, No. 1, 1991, pp. 31–39.

[4]Morgan, R. G., "Superorbital Expansion Tube," *Proceedings of 21st International Symposium on Shock Waves*, Vol. 1, Panther, Fyshwick, Australian Capital Territory, Australia, 1998, pp. 71–76.

[5]Sasoh, A., Ohnishi, Y., Ramjaun, D., Takayama, K., Otsu, H., and Abe, T., "Effective Test Time Evaluation in High-Enthalpy Expansion Tube," *AIAA Journal*, Vol. 39, No. 11, 2001, pp. 2141–2147.

[6]Otsu, H., Suzuki, K., Fujita, K., and Abe, T., "Radiative Heating Analysis Around the MUSES-C Reentry Capsule at a Superorbital Speed," AIAA Paper 98-2447, June 1998.

[7]Otsu, H., Suzuki, K., Fujita, K., and Abe, T., "Effect of Ablative Gas on the Radiative Environment Around the MUSES-C Reentry Capsule," AIAA Paper 99-3463, June 1999.

[8]Park, C., "Assessment of Two-Temperature Kinetic Model for Ionizing Air," *Journal of Thermophysics and Heat Transfer*, Vol. 3, No. 3, 1989, pp. 233–244.

[9]Gnoffo, P. A., Gupta, R. N., and Shinn, J. L., "Conservation Equations and Physical Models for Hypersonic Air Flows in Thermal and Chemical Nonequilibrium," NASA TP-2867, 1989.

[10]Park, C., "Assessment of Two-Temperature Kinetic Model for Dissociating and Weakly Ionizing Nitrogen," *Journal of Thermophysics and Heat Transfer*, Vol. 2, No. 1, 1988, pp. 8–16.

[11]Millikan, R. C., and White, D. R., "Systematics of Vibrational Relaxation," *Journal of Chemical Physics*, Vol. 39, No. 12, 1963, pp. 3209–3213.

[12]Sharma, S. P., Huo, W., and Park, C., "The Rate Parameters for Coupled Vibration-Dissociation in Generalized SSH Theory," AIAA Paper 88-2714, 1988.

[13]Park, C., *Nonequilibrium Hypersonic Aerothermodynamics*, Wiley, New York, 1990, p. 108.

[14]Gupta, R. N., Yos, J. M., Thompson, R. A., and Lee, K.-P., "A Review of Reaction Rates and Thermodynamic and Transport Properties for an 11-Species Air Model for Chemical and Thermal Nonequilibrium Calculations to 30,000 K," NASA RP-1232, 1990.

[15]Vincenti, W. G., and Kruger, C. H., Jr., *Introduction to Physical Gas Dynamics*, Krieger, Malabar, FL, 1965, p. 21.

[16]Candler, G. V., and MacCormack, R. W., "The Computation of Hypersonic Ionized Flows in Chemical and Thermal Nonequilibrium," AIAA Paper 88-0511, Jan. 1988.

[17]Wilke, C. R., "A Viscosity Equation for Gas Mixtures," *Journal of Chemical Physics*, Vol. 18, No. 4, 1950, p. 517.

[18]Liou, M.-S., and Steffen, C. J., "A New Flux Splitting Scheme," *Journal of Computational Physics*, Vol. 107, No. 1, 1993, pp. 23–39.

[19]Wada, Y., and Liou, M.-S., "A Flux Splitting Scheme with High-Resolution and Robustness for Discontinuities," AIAA Paper 94-0083, Jan. 1994.

[20]Bussing, T. R. A., and Murman, E. M., "Finite-Volume Method for the Calculation of Compressible Chemically Reacting Flows," *AIAA Journal*, Vol. 26, No. 9, 1988, pp. 1070–1078.

[21]Eberhardt, S., and Imlay, S., "Diagonal Implicit Scheme for Computing Flows with Finite Rate Chemistry," *Journal of Thermophysics and Heat Transfer*, Vol. 6, No. 2, 1992, pp. 208–216.

[22]Fujita, K., Abe, T., and Suzuki, K., "Air Radiation Analysis of a Super-orbital Reentry Vehicle," AIAA Paper 97-2561, June 1997.

M. Sichel
Associate Editor